2008 IEEE International Conference on
Robotics and Automation
Pasadena, CA, USA, May 19-23, 2008

Design of a Mobile Mechanism Possessing Driving Ability and Detecting Function for In-Pipe Inspection

Peng Li, Shugen Ma, *Member, IEEE*, Bin Li and Yuechao Wang

***Abstract*—In this paper, a mobile mechanism with driving capability and detecting function is proposed for in-pipe inspection task. Based on this mechanism, a robot is designed and fabricated. The advantage of this robot is that it has mobile ability in the pipe and detecting function for inspection, while only one DC motor is installed. This results in low energy consumption and low cost to make. The robot propels itself in the pipe under a driving mode, and it is used for finding the defect of the pipe under a detecting mode. By switching these two working modes, the robot performs the inspection task without other extra DC motors. Moreover, a velocity change mechanism is introduced to adapt the change of the payload through adjusting the incline angle of the roller. The characteristics of this mechanism are analyzed by comparison with a classical screw drive robot and a direct drive robot. Finally, basic experiments are conducted to testify the mobility and efficiency of this robot.**

I. Introduction

PIPELINES have been used in many countries for the transportation of liquids and gases for decades. Now, the pipelines should be monitored since they are aging. Some problems, such as cracks, leakages and damages by other reasons, should be detected as early as possible in order to prevent serious accidents. Many pipe inspection robots have been developed for the inspection tasks. Hayashi *et al*. developed a pipe robot that employed an external motor to drive itself [1], [2]. Hirose *et al*. reported the THES series robots for the inspection of gas pipes [3]. Toshiba Corporation developed a micro robot equipped with a high resolution camera and a pair of pneumatic hands for checking the 1-in pipe [4]. MRINPECT3 developed by Choi and Ryew employed the link-type configuration [5]. Roh developed MRINSPECT4, a wheel type robot based on differential drive [6]. A wheel type robot developed by Oya had steering ability by adding driving motors to the wheel joints [7]. Zhu reported his pipe robot used for sampling in the sewage pipe [8]. Zagler and Peiffier developed a walking type pipe robot that equipped sixteen motors on eight legs for moving [9].

As seen, the pipe robots are usually equipped with many motors that have different functions to execute the inspection task. For example, some motors are used for driving the robot, while other motors may be used for positioning the sensor or other devices for detecting the inner surface of the pipe. Because so many motors are used, the robots consume too much energy. For this reason, the operation time to perform a task is reduced and the cost of making a robot increased.

In this paper, we propose a new mobile mechanism that reduces the number of the driving motors, while the robot still has the mobile ability and inspecting function. That is, we are trying to increase the working efficiency of the driving motor and decrease the cost of the pipe inspection robot. Moreover, a velocity change mechanism that endows the robot with adaptability to the payload on the robot body is introduced. Thus, the new robot imposes low requirements to the power supply, and it is a low cost robot. The following section introduces the concept of the new robot. Section III shows the design of the robot, and the mechanism of the new robot is analyzed in section IV. Section V gives the results and experiments. Finally, we offer the conclusion at present.

II. Concept of The New Mobile Mechanism

Since the pipe environment is not always fixed, a pipe robot needs adaptability to the environment. Furthermore, the pipe robot should not only have the mobility but also carry devices for inspection. The narrow space constrains the robot's size, so the robot must make full use of the capacity of the motor. Therefore, an in-pipe robot should possess the characteristics: multifunction, adaptability and efficiency.

The speed of the wheel type robots is easy to reach a high level, and their traction force can be increased through enhancing the normal force and the adhesion coefficient between the wheel and the inner surface of the pipe. The wheel type drive is thus always employed as the main driving method for in-pipe robot and is widely used from small to large pipes, compared to other driving methods.

Wheel type robots can also be divided into Direct Drive Wheel type robots (DDW) and Screw Drive Wheel type robots (SDW). As shown in Fig.1(a), the wheel orientation of the DDW is parallel to the axis of the pipe. The motors drive the wheels directly or via the transmission mechanism. The transmission is used to reduce the speed of the motor or change the orientation of the velocity produced by the motors.

Manuscript received August 18, 2007. This work is supported by The National High Technology Research and Development Program of China (863 Program) (2006AA04Z230).

Peng Li is with the State Key Laboratory of Robotics, Shenyang Institute of Automation, Chinese Academy of Sciences, Shenyang 110016, China. He is also with the Graduate School of the Chinese Academy of Sciences, Beijing 100039, China. (e-mail: lipeng@sia.cn; lipeng.bird@gmail.com).

Shugen Ma is with the Organization for Promotion of the COE Program, Ritsumeikan University, Shiga-ken 525-8577, Japan. He is holding professor position at Shenyang Institute of Automation, Chinese Academy of Sciences, Shenyang 110016, China. (e-mail: shugen@fc.ritsumei.ac.jp).

Bin Li and Yuechao Wang are with the State Key Laboratory of Robotics, Shenyang Institute of Automation, Chinese Academy of Sciences, Shenyang 110016, China. (e-mail: libin@sia.cn ycwang@sia.cn).

As shown in Fig.1(b), the Screw Drive Wheel type robot is usually composed of a rotator, elastic support arms, rollers and a motors for driving. The rollers have an incline angle with respect to the cross section of the pipe. When the motor turns, the rollers rotate not only with their own axes but also around the axis of the pipe. Then the whole body moves forward. If the motor turns reversely, the body moves backward.

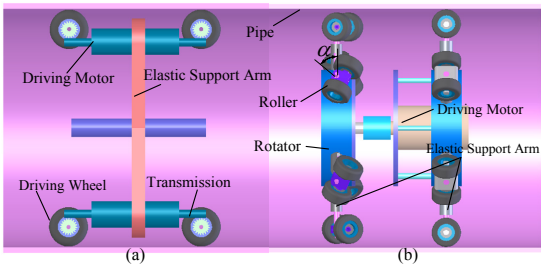

Fig. 1. Wheel type pipe robot. (a) Direct drive wheel type robot. (b) Screw drive wheel type robot.

The Screw drive wheel type robot needs less driving motors, which results in less power consumption and more working time to operate tasks. This type of robot also simplifies the control complexity, compared with other driving methods.

The proposed robot shown in Fig. 2 is based on the screw drive principle, and the robot not only has the mobile ability but also has the inspection ability in the pipe, while only one DC motor is used. This mobile mechanism is composed of a driving rotator, driving arms, rollers, a detecting rotator, a stator, support arms and a driving motor.

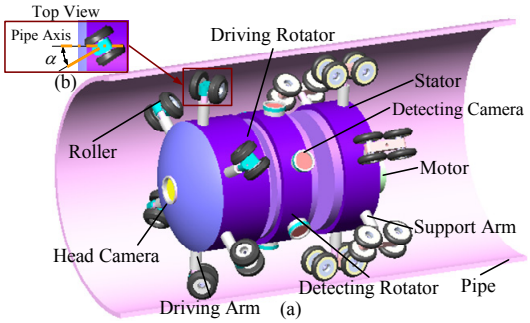

Fig. 2. Concept of the new robot. (a) Structure of the robot. (b) Top view of the roller.

The driving arms are fixed each 60 degrees on the periphery of the driving rotator. The rollers on the driving arms have an incline angle with respect to the axis of the pipe and are pressed onto the inner surface of the pipe. The advantage of the driving arm is that the roller changes its incline angle when the resistance force is altered, and the speed of the robot changes due to the change of the incline angle. This is a Velocity Change Mechanism (VCM). The detecting rotator rotates with respect to the axis of the pipe and is mounted with cameras that are used for executing the inspection task. When the detecting rotator turns, the cameras will monitor the periphery of the pipe's inner surface to find the pipe's problems. One driving motor is attached on the stator and support arms that prevent the stator from rolling around the axis of the pipe.

The only one motor fixed on the stator provides both torque of the driving rotator and that of the detecting rotator. Therefore, the number of the driving motor is reduced but the robot still has the mobile ability and detecting function, and the VCM endows the robot with adaptability to the payload.

III. Mechanical Design of The Robot

A. *Mechanism with Driving and Detecting Functions*

Because the new robot only uses one motor to drive in the pipe and executes inspection task, the transmission mechanism should be considered carefully before the mechanism is designed. The requirements are as follows:

1) Mobile mechanism for traveling in pipe is necessary.
2) Part of the robot can be used as the base of the electronic devices that are used for inspection.
3) One DC motor is used to achieve mobile and detecting ability of the robot.

The mechanism designed for the robot should satisfy the above requirements. Fig. 3 illustrates the configuration of the mechanism in detail. The principle of this mechanism is that the power of the motor is transmitted via a coupling to the spur gear 1 and the gear 2. When the motor and the spur gear rotate, the coupling eliminates the offset between them. The spur gear 2 and the sun gear are fixed on the central axis. When the central axis turns, the power of the motor is transmitted to the ring gear, and then the ring gear rotates the driving arms that are fixed on the periphery of the ring gear. This is one route of the power output.

Another power output route is that when the motor is activated, the power is transmitted to the central axis and turns the sun gear, which turns the planet gears. Finally, the power of the motor is transferred to the planet gear carrier, which is used as the base of the detecting devices. The rollers mounted on the driving arms and the supporting arms are pressed by the force of the compressed springs. Moreover, the roller on the driving arms has an incline angle with respect to the axis of the pipe, and this angle changes when the payload of the robot varies.

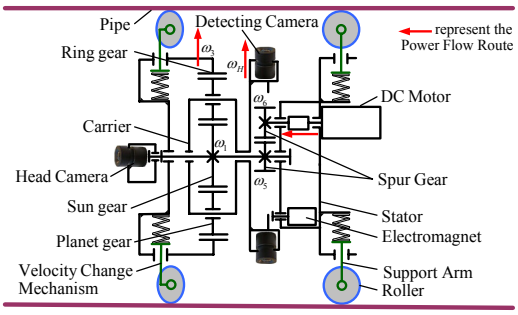

Fig. 3. Mobile mechanism of the robot.

A switching electromagnet that is on the stator always

exerts constrains to the planet carrier. As a result, if the motor works, the driving arms are activated, while the planet carrier is not. On the contrary, if the electromagnet is electrified, the constrained force on the planet carrier disappears. When the motor rotates, the planet carrier turns, and the driving arms keep still.

Let ω_6, ω_3 and ω_H denote the angular velocity of the spur gear 1, the ring gear and the planet gear carrier of the mechanism in Fig. 3 respectively. i_{16} denotes the reduction ratio from the sun gear to the spur gear 1, while K is the ratio of teeth of the ring gear to that of the sun gear. We thus obtain the following equation

$$i_{16}\omega_6 + K\omega_3 = (K+1)\omega_H \tag{1}$$

From (1), if $\omega_H = 0$, we obtain the reduction ratio from the spur gear 1 to the ring gear, i_{63}, is equal to $i_{61}K$; when $\omega_3 = 0$, the ratio from the spur gear 1 to the planet gear carrier, i_{6H}, is equal to $i_{61}(K+1)$. Here,

$$\begin{aligned} i_{61} &= \omega_6/\omega_1 = z_5/z_6 \\ i_{63} &= \omega_6/\omega_3 = i_{61}K \\ i_{6H} &= \omega_6/\omega_H = i_{61}(K+1) \\ K &= z_3/z_1 \end{aligned} \tag{2}$$

Where i_{ij} denotes the transmission ratio from the ith part to the jth part, while ω_i and z_i represent the angular velocity and number of teeth of the ith gear respectively. Consequently, the mobile mechanism has two working modes, whose ratios of transmission are different from each other.

B. Velocity Change Mechanism

As mentioned above, the driving arm fixed on the ring gear can change its incline angle according to the payload of the robot. The driving arm is realized by the mechanism in Fig. 4.This mechanism is composed of a rolling block, a rolling rod, a sliding rod, pins, fender blocks, a container, a spring, a gasket, an adjustive blot, and wheels. The sliding rod has a concave, while the rolling rod has a convex. The sliding rod, which can only move along with the slot on the container, is pressed on the rolling rod, on which the rolling block is fixed, by the spring. When the rolling rod rotates against the sliding rod, a resistant torque that is generated by the convex/concave set prevents this motion trend. That is, to slant the rolling rod an angle(change the incline angle), there must exist a moment to conquer the resistant torque, otherwise, the incline angle does not change. A pin and a fender block are attached on the rolling rod and the sliding rod, which are used to limit the relative position between the rolling rod and sliding rod. A gasket and an adjustive blot that are used for setting the initial force of the spring are arranged at the bottom of the spring.

Zhu used trapezoid shape wheels to keep the robot from rotating around the axis of the pipe [8]. Here, we use the trapezoid shape wheels for increasing the contact area, when the robot surmounts the obstacle.

The incline angle of the roller on the driving arm has influence on the translated velocity of this type robot (see next section). If the angle varies, which means the concave/convex set relative position changes, according to the payload exerted on the robot, the velocity of the robot will change with the payload. That means if the payload increases, the velocity of the robot will decrease.

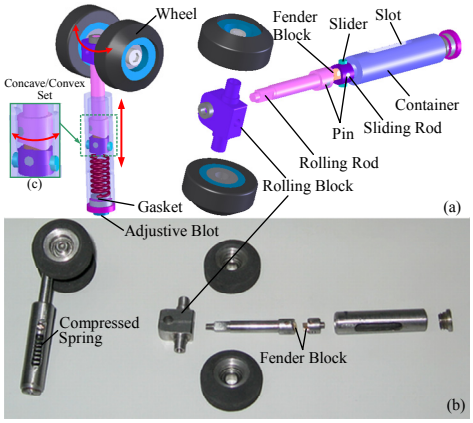

Fig. 4. Velocity change mechanism. (a) Detailed structure of the VCM. (b) Prototype of the VCM. (c) Zoom in the concave/convex set.

C. Working Mode of The Robot

The proposed robot has two typical working modes, as seen Fig. 5.

1) Driving Mode: Under the driving mode, the driving motor rotates the driving arms, while the planet carrier does not turn because of the constrained force exerted by the switching electromagnet. Thus, the rotating arms generate traction force to propel the robot forward or backward. The ratio of the driving mode i_{63} is less than i_{6H}, so the robot travels quickly under this mode, as shown in Fig. 5(a).

2) Detecting Mode: When electromagnet is electrified, the constraint acting on the planet carrier disappears. The motor turns the planet carrier rather than the driving arms. Therefore, the robot uses the detecting device to check the defects of the inner surface of the pipe, as shown in Fig. 5(b).

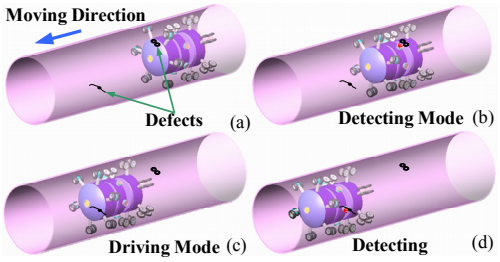

Fig. 5. Two working modes of the robot.

After checking the area, the robot is back to the driving mode again and goes on moving to reconnoitre other suspicious area, as shown in Fig. 5(c) and (d).

Although the robot is equipped with one DC motor, it has both mobile ability and inspection ability. With the driving motors' number decreasing, the power consumption and the cost of the robot drop and the working efficiency of the

driving motor is increased.

D. Front Camera Installation

A CMOS camera module is installed at the head of the robot for inspection. The posture of robot body is changing more or less for most of in-pipe robots, so the camera module can not be installed to the robot body directly. To solve this problem, a mechanism in Fig.6 is proposed. The gear1 is fixed on the central axis of the robot, and the camera frame can rotate around the central axis, and the gear 2 can rotate around its own axis that is fixed on the camera frame. When this mechanism is disturbed by other factors and slants a small angle θ, the mechanism returns to its balance position all by itself. Thus, the change of the robot's posture does not affect that of the orientation of the camera. The camera is wireless, which avoids the problem of twisting the signal cable.

Fig. 7(a) shows the raw image captured from the head camera and Fig. 7(b) shows that a hole with 2mm is detected by the detecting camera.

A prototype based on the proposed mechanism has been fabricated, which is shown in Fig. 8. Main parameters of the robot are listed in table I.

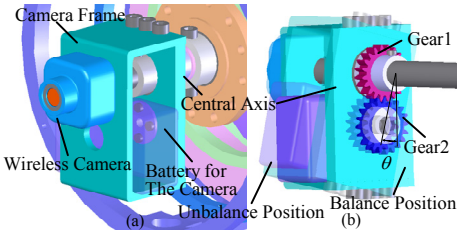

Fig. 6. Installation of the camera system. (a) Front view. (b) Back view.

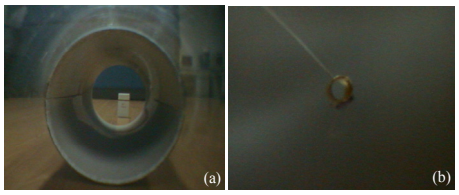

Fig. 7. Raw image from the cameras. (a) Image from the head camera. (b) Image from the detecting camera.

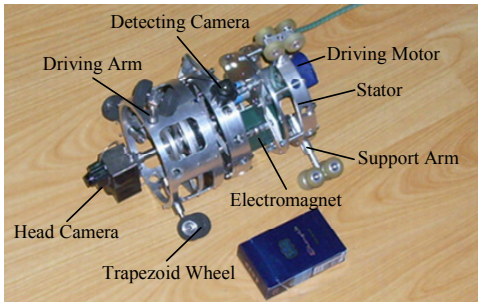

Fig. 8. Prototype of the proposed robot.

TABLE I
SPECIFICATIONS OF THE NEW ROBOT

Max-Min Diameter	205~175mm
Total Weight(with camera)	1.95Kg
Ratio of Transmission	2(driving mode), 3(detecting mode)

IV. ANALYSIS OF THE NEW ROBOT WITH THE DIRECT DRIVE ROBOT

A. Kinematics

The inner diameter of pipe is D, as shown in Fig. 9. C denotes the centroid of the robot, and O_i denotes the center of the roller on the driving arms or the driving wheel. Point C_1 denotes the rolling centre of O_i with respect to the axis of pipe. Orthogonal unit vector $\boldsymbol{i}$, $\boldsymbol{j}$ and $\boldsymbol{k}$ are defined at the centroid of the robot, and Q denotes the contact point between the rollers or wheels and pipe. Orthogonal unit vectors $\boldsymbol{h}_i$, $\boldsymbol{g}_i$ and $\boldsymbol{k}_i$ are fixed to the centre of the roller or driving wheel, and α denotes the incline angle of $\boldsymbol{h}_i$ with respect to the cross section of pipe.

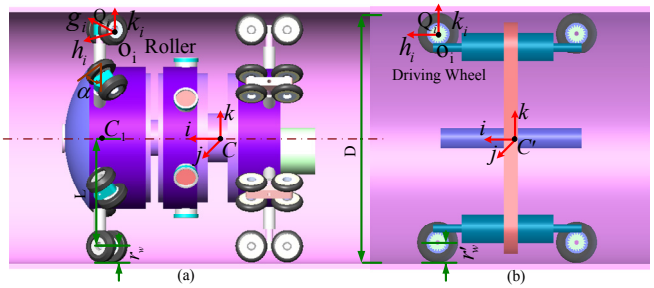

Fig. 9. Kinematic model. (a) Model of the screw drive type pipe robot. (b) Model of the direct drive type pipe robot.

In Fig. 9(a), $\dot{\boldsymbol{r}}_c$ and $\dot{\boldsymbol{o}}_i$ denote the velocity of C, and O_i. $\boldsymbol{v}_{cc_1}$ and $\boldsymbol{v}_i$ is the relative velocity of C with respect to C_1 and the relative velocity of C_1 with respect to O_i. $\boldsymbol{\omega}_{12}$ is the relative angular velocity of the driving arm with respect to the stator, ω_3 is the scalar angular velocity of the driving arm, and $\dot{\varphi}_i$ is the ith scalar angular velocity of the roller on the driving arm, respectively. If the direction of the angular velocity is clockwise looked from the head of the robot, it will be a negative value. Otherwise, it will be positive. r_w is the radius of the roller. The velocity relations of the robot are as follows

$$\dot{\boldsymbol{r}}_c = \dot{\boldsymbol{o}}_i + \boldsymbol{v}_i + \boldsymbol{v}_{cc_1} \tag{3}$$

$$\dot{\boldsymbol{o}}_i = \left(\boldsymbol{\omega}_{12} + \dot{\varphi}_i \boldsymbol{g}_i\right) \times \boldsymbol{r}_w \tag{4}$$

$$\boldsymbol{v}_i = \boldsymbol{\omega}_{12} \times \overrightarrow{O_i C_1} \tag{5}$$

$$\boldsymbol{\omega}_{12} = -\omega_3 \boldsymbol{i} \tag{6}$$

The relationship between $\boldsymbol{h}_i$, $\boldsymbol{g}_i$ and $\boldsymbol{i}$, $\boldsymbol{j}$ is

$$\begin{bmatrix} \boldsymbol{h}_i \\ \boldsymbol{g}_i \end{bmatrix} = \begin{bmatrix} \sin\alpha & \cos\alpha \\ \cos\alpha & -\sin\alpha \end{bmatrix} \begin{bmatrix} \boldsymbol{i} \\ \boldsymbol{j} \end{bmatrix} \tag{7}$$

From (3) to (7), the velocity of screw drive type is given by

$$\dot{\boldsymbol{r}}_c = \omega_3 \left(r_w + L\right) \tan\alpha \boldsymbol{i} \tag{8}$$

In Fig.9(b), when the direct drive robot is moving in the straight pipe, its velocity $\dot{\boldsymbol{r}}_c'$ is

$$\dot{\boldsymbol{r}}_c' = \omega_w r_w \boldsymbol{i} \tag{9}$$

Where ω_w is the scalar angular velocity of the driving wheel.

B. Velocity-load Relationship

In Fig.10(a), F_{dj} represents the friction force along the normal direction, and F_{rj} represents the friction force along the tangential direction. The superscript, such as (1) and (2), denotes the corresponding value at different positions or postures. F_{re} denotes the sum of all the other resistant forces, and M_{drive} is the driving torque acting on the robot. n is the number of the driving arms. Now, we obtain

$$n\left(F_{dj}^{(1)}\cos\alpha - F_{rj}^{(1)}\sin\alpha\right) = F_{re}^{(1)} \tag{10}$$

$$n\left(F_{dj}^{(1)}\sin\alpha + F_{rj}^{(1)}\cos\alpha\right) = M_{drive}^{(1)} / 0.5D \tag{11}$$

From (10) and (11),

$$\frac{f_n\cos\alpha - f_t\sin\alpha}{f_n\sin\alpha + f_t\cos\alpha} = \frac{0.5DF_{re}^{(1)}}{M_{drive}^{(1)}} \tag{12}$$

Where f_n and f_t is the friction coefficient in the normal direction and tangential direction respectively.

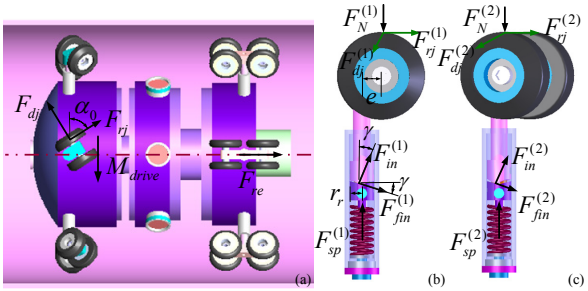

Fig. 10. Forces acting on the robot. (a) Forces a on the main body. (b) Forces on the driving arm. (c) The forces slant the wheel an angle of $\Delta\alpha$.

In Fig. 10(b),

$$2\left(F_{in}^{(1)}\cos\gamma - F_{fin}^{(1)}\sin\gamma\right) = F_{sp}^{(1)} \tag{13}$$

$$2\left(F_{in}^{(1)}\sin\gamma + F_{fin}^{(1)}\cos\gamma\right)r_r = F_{dj}^{(1)}e \tag{14}$$

Where F_{in} is the contact force between the rolling rod and the sliding rod, F_{fin} is the friction force due to F_{in}, F_{sp} is the force of spring, γ is the angle of the contact mate, r_r is the radius of the rod, e is the offset, and f_c is the friction coefficient of the contact mate, respectively.

$$\frac{\left(\cos\gamma - f_c\sin\gamma\right)}{\left(\sin\gamma + f_c\cos\gamma\right)r_r} = \frac{F_{sp}^{(1)}}{F_{dj}^{(1)}e} \tag{15}$$

Fig. 10(c) shows that the rolling rod turns an angle of $\Delta\alpha$. So

$$F_{sp}^{(2)} = F_{sp}^{(1)} + 2kr_r\tan(\gamma)\Delta\alpha/\pi \tag{16}$$

Then, the incline angle at this time is

$$\alpha = \alpha_0 - \Delta\alpha \tag{17}$$

Thus, equation (8), (10)-(12) should be updated by (17).

Considering of the driven character of a DC motor, we obtain

$$n_m = n_0 - gM_m \tag{18}$$

Where n_m is the speed of the motor, and n_0 is the speed under free load. M_m is the torque generated by the motor, while g is defined as $\Delta n_m / \Delta M_m$.

Let $i_{total} = i_m i_t$ and $\eta = \eta_m\eta_t$. Here, i_m and i_t denote the transmission ratio of the motor reduce head and transmission of the robot respectively. η_m and η_t denote the efficiency of the motor reducer head and transmission of the robot. n_{drive} and M_{drive} are the speed and torque acting on the driving arms and the driving wheels.

$$n_{drive} = n_0 / i_{total} - gM_{drive} / i_{total}^2\eta \tag{19}$$

Now, we substitute (19) into (8), the velocity- load character of the new robot is derived as

$$\dot{\boldsymbol{r}}_c = \pi(r_w + L)\tan(\alpha_0 - \Delta\alpha)(n_0 / i_{total} - gM_{drive} / i_{total}^2\eta)/30\boldsymbol{i} \tag{20}$$

For the direct drive pipe robot, the torque acting on the wheel can be written as

$$M'_{drive} / r_w = F'_{re} \tag{21}$$

Substitute (19) and (21) into (9)

$$\dot{\boldsymbol{r}}'_c = \pi r_w(n_0 / i_{total} - gM'_{drive} / i_{total}^2\eta)/30\boldsymbol{i} \tag{22}$$

Equation (22) is the velocity-load character of the direct drive type pipe robot.

C. Computer Simulation

The parameters are set as follows: n=3, $\gamma = 20^\circ$, r_r=4mm, e=3mm, k=0.5N/mm, $F_{sp}^{(1)}$ =5N, while same parameters of motor and transmission are used for different kinds of robots. The driving motor parameters are listed in table II [10]. Other parameters are set as: i_t=3, η_t =0.75, r_w=10mm, and the environment parameters are D=190mm, f_n=0.5, f_t=0.01, f_c =0.25.

TABLE II
PARAMETERS OF THE MOTOR

V_{rated}=24v	n_0=5390rpm	n_{max}=7300rpm
g=103rpm/mNm	η_m =0.8	i_m=199

Fig. 11 gives the comparison of the robot with velocity change mechanism (VCM) and the classical screw drive robot, where the angle of the roller is 20°. It is known that the angle decrease with respect to the payload increase in the proposed mechanism, while there is no any change in the classical screw drive robot.

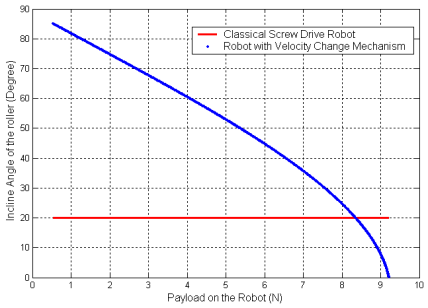

Fig. 11. Payloads-incline angle relation.

Fig. 12(a), (b) and (c) give the comparisons of the screw drive robot with velocity change mechanism, the screw drive robot with a constant angle of 20°, and a direct drive robot, while Fig.12(d) shows velocity-payload calculation at different speed of the proposed screw drive robot. From the

results, it is known that when the same payload acts on the robots, robot with velocity change mechanism moves faster.

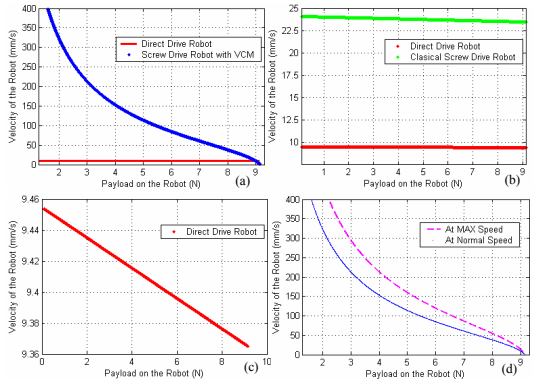

Fig. 12. Comparisons of the screw drive type and the direct drive type robots. (a) Velocity-payload relation of the screw drive robot with VCM and the direct drive robot, while $\Delta\alpha$ varies from 0° to 77.4°. (b) Velocity-payload relation of the screw drive robot with a constant incline angle of 20° and the direct drive robot. (c) Driving characteristics of the direct drive robot. (d) Velocity-payload calculation at different speed of the screw drive robot with VCM.

V. Experiments

To confirm the mobility of the proposed mechanism, experiments have been conducted. The environment is a pipe with diameter of 200mm that has a hole defect. The head camera and the detecting camera are attached on the robot as the vision system for inspection. Fig.13(a) shows that the robot propels in pipe under the driving mode, while the robot stops to check the defect area using the camera on the detecting rotator in Fig.13(b). The robot goes on propelling, as seen in Fig.13(c) and (d). Fig. 13(e) shows the robot is examining a small hole whose image is in Fig. 7(b).

In Fig. 14, the environment is composed of pipes with different diameters and a concentrically step is formed at the conjunction of the two pipes. Fig. 14(a) and (b) shows that the robot moves in the larger pipe, and the robot is checking the suspicious area in Fig.14(c) under the detecting mode. In Fig.14(d), the robot is overcoming the concentric step with the height of 5mm using its trapezoid shape wheels. Finally, the robot entered in the smaller pipe entirely.

VI. Conclusion

A new mobile mechanism for in-pipe inspection robot has been proposed in this paper. The prototype has both mobile ability and checking function for inspection while only one DC motor is equipped. This makes the robot be efficient in low energy consumption and low cost to make. The robot moves in the pipe under the driving mode, and it can find the defect of the pipe under the detecting mode without using any extra motors. Furthermore, velocity change mechanism has also been introduced and the performance of the robot equipped with this mechanism has been analyzed. Simulation shows the mechanism has the adaptability to the payload. Finally, the mobility of the robot and its efficiency have been confirmed by the experiments as well.

References

[1] S. Iwashina, I. Hayashi, N. Iwatsuki, and K. Nakamura, "Development of In-Pipe Operation Micro Robots," in *Proc. Int. Symp. Micro Machine, Human Science*, 1994, pp. 41-45.

[2] I. Hayashi, N. Iwatsuki, and S. Iwashina, "The running characteristics of a screw-principle microrobot in a small bent pipe," in *Proc. Int. Symp. Micro Machine, Human Science*, 1995, pp. 225-228.

[3] S. Hirose, H. Ohno, T. Mitsui, and K. Suyama, "Design of in-pipe inspection vehicles forφ25,φ50,φ150 pipes," in *Proc. IEEE Int. Conf. Robotics, Automation*, 1999, pp. 2309-2314.

[4] K.Suzumori, T.Miyagawa, M.Kimura, Y.Hasegawa, "Micro Inspection Robot for 1-in Pipes," *IEEE/ASME Trans. Mechatronics*, vol. 4, no. 3, pp. 286-292, 1999.

[5] H.R. Choi, and S.M. Ryew, "Robotic system with active steering capability for internal inspection of urban gas pipelines," *Mechatronics*, vol. 12, pp. 713-736, 2002.

[6] S.G. Roh, and H.R. Choi, "Differential-drive in-pipe robot for moving inside urban gas pipelines," *IEEE Trans. Robotics*, vol. 21, no. 1, pp. 1-17, 2005.

[7] T. Oya, and T. Okada, "Development of a steerable, wheel-type, in-pipe robot and its path planning," *Advanced Robotics*, vol. 19, no. 6, pp. 635-650, 2005.

[8] C. Zhu, "In-pipe robot for inspection and sampling tasks," *Industrial Robot: An International Journal*, vol. 34, no. 1, pp. 39-45, 2007.

[9] A. Zagler, and F. Pfeiffer, ""MORITZ" a pipe crawler for tube junctions," in *Proc. IEEE Int. Conf. Robotics, Automation*, 2003, pp. 2954-2959.

[10] *Maxon Motor Catalog*, Maxon motor Co., Ltd. 2004, p.115.

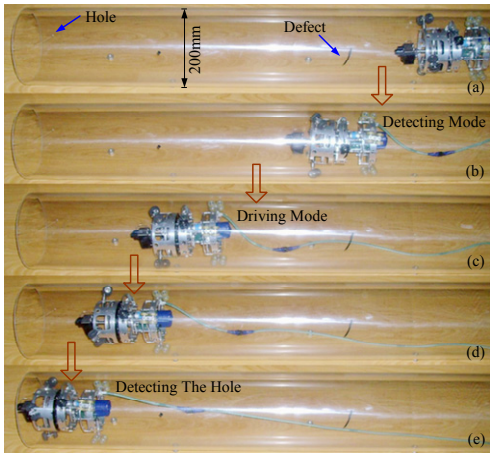

Fig. 13. Test of the proposed mechanism.

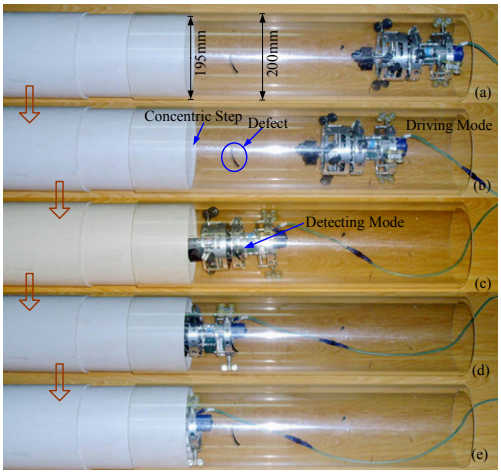

Fig. 14. Concentric step surmounting experiment.